ELSEVIER

Journal of Structural Geology 26 (2004) 2011–2023

JOURNAL OF STRUCTURAL GEOLOGY

www.elsevier.com/locate/jsg

Experimental grain size-sensitive flow of hot-pressed Brazilian quartz aggregates

E.H. Rutter*, K.H. Brodie

Rock Deformation Laboratory, Department of Earth Sciences, University of Manchester, Manchester M13 9PL, UK

Received 4 September 2003; received in revised form 24 April 2004; accepted 25 April 2004

Available online 2 July 2004

Abstract

Grain size-sensitive flow may be of particular importance in the flow of rocks in natural high-strain zones. Hot-pressed aggregates of synthetic, ultrafine-grained Brazilian quartz of nominal grain sizes 0.4, 1.3 and 4.5 μm were deformed at 300 MPa confining pressure and temperatures of 1273–1473 K. Fully ductile flow at differential stresses below 200 MPa followed $\dot{\epsilon} = 0.4\sigma\exp(-220000/RT)/d^2$ where $\dot{\epsilon}$ is strain rate (s^{-1}), σ is stress (MPa), d is grain size (microns) and R is the gas constant. Grains remained equant and mostly dislocation-free, without significant crystallographic fabric. Water pressure (~25–50 MPa) was estimated from water adsorbed onto grain boundaries during specimen fabrication. Flow was inferred to be controlled by silicon volume diffusion and to be sensitive to water fugacity. At differential stresses >200 MPa non-linear flow involved dislocation motion. Extrapolation to natural strain rates and temperatures that predict grain-size sensitive flow in quartz should only be important at >800 K and very small grain sizes (~1 μm). Flow law parameters may change over the extrapolation interval, e.g. through a transition to control by silicon grain-boundary diffusion, but geological evidence suggests that flow of even very fine-grained quartzites commonly occurs by recrystallization-accommodated dislocation creep, rather than by diffusional accommodation.

Keywords: Grain size-sensitive flow; Quartzite; Experimental deformation

1. Introduction

Grain size-sensitive flow, in which the flow stress decreases with decreasing grain size, is believed to be of particular importance in natural rock deformation. It is commonly observed that localized high strain zones in natural rocks deformed at high temperatures, which by inference are zones of mechanical weakness, are also zones of tectonic grain size reduction, and therefore places in which this type of flow might dominate. There are several processes that can lead to tectonic grain size reduction and potentially to flow stress sensitivity to grain size. These are dynamic recrystallization, cataclasis and formation of new, fine grains as metamorphic reaction products. The study of grain size reduction with progressive strain poses the technical difficulty of making accurate mechanical measurements over a wide range of strain, until a steady state condition is reached. However, the separate issue of the rheology of rocks after the grain size reduction has been achieved can be addressed, at least in part, by mechanical tests on specimens of a range of controlled grain sizes, fabricated by hot isostatic pressing. We have previously taken this approach to investigate grain size-sensitive flow of calcite rocks (Walker et al., 1990; Rutter et al., 1994), and others have done the same with olivine rocks (Karato et al., 1986; Hirth and Kohlstedt, 1995; McDonnell et al., 1999; Mei and Kohlstedt, 2000), anhydrite rock (Dell'Angelo and Olgaard, 1995), feldspar rocks (Tullis and Yund, 1991; Dimanov et al., 1999; Rybacki and Dresen, 2000) and ice (Goldsby and Kohlstedt, 2001).

In this paper we describe experiments on hot-pressed samples fabricated from powders prepared from clear, Brazilian quartz crystals, of starting nominal grain sizes 0.4, 1.3 and 4.5 μm. Grain-size sensitive flow has been demonstrated in these experiments provided the intergranular water content of the sample was too small to favour grain growth.

* Corresponding author. Fax: +44-161-2753947.
E-mail address: e.rutter@man.ac.uk (E.H. Rutter).

0191-8141/$ - see front matter © 2004 Elsevier Ltd. All rights reserved.
doi:10.1016/j.jsg.2004.04.006

2. Sample preparation and characterization

The polycrystalline samples used in this study were prepared by hot isostatic pressing (HIP) of crushed single crystals of natural Brazilian quartz that were clear and free from optically visible fluid inclusions. Selected crystals were crushed into fragments up to a few millimetres across, and all visible contaminants were removed by hand picking. The remaining material was washed in hydrochloric acid and rinsed with distilled water before crushing in a TEMA tungsten carbide mill. The size fraction less than 64 μm was separated by sieving, and separated into three sub-fractions of modal grain diameters of 0.4, 1.3 and 4.5 μm by centrifuging in water. Particle size distributions were determined by laser particle sizer (Fig. 1). Specimens prepared from each of the size fractions will be referred to by these initial modal sizes. The finest fraction was collected by settling from large volumes of water. All samples were dried in an oven at 90 °C and stored in glass bottles.

The particle size distributions (by volume) are all significantly skewed, so that the mean particle sizes differ from the modes. The means are respectively 0.65 ± 0.3, 1.1 ± 0.3 and 5.5 ± 3.5 μm, where the ± figures are the standard deviations of each distribution curve, and thus properties of the distribution rather than standard errors on the means. There is a substantial overlap of particle sizes between samples, which potentially can lead to a lack of clear distinction in the mechanical behaviour of specimens prepared from the different fractions. Further, a wide spread of particle sizes potentially can lead to dominance by different deformation mechanisms in different size sub-fractions in a single specimen (Freeman and Ferguson, 1986). On the other hand, to produce different sized fractions without significant overlap necessarily requires widely different mean particle sizes, and this in turn can mean that grain size-sensitive flow might not be accessed in test pieces prepared from all size fractions. Any suite of specimens prepared to study grain size-sensitive flow is necessarily a compromise in these respects. The same starting materials were used in the study of intracrystalline deformation of hot-pressed Brazilian quartz reported by Rutter and Brodie (2004), and the results of the sample characterization reported in that paper are only briefly summarized below.

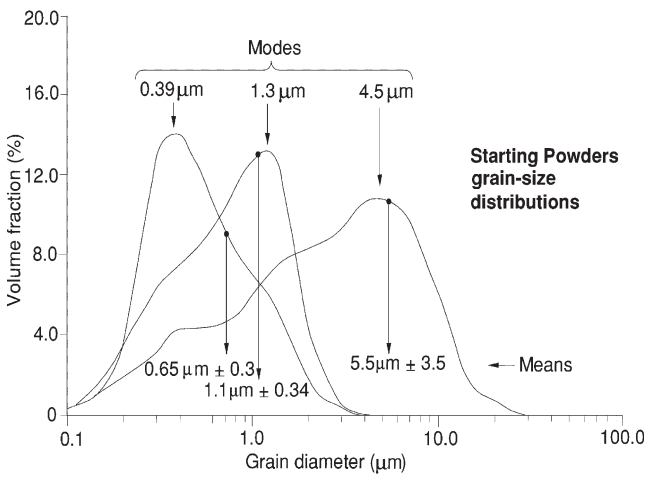

Fig. 1. Particle size distributions for the starting quartz powders, measured by laser particle sizer. ± figures shown with mean sizes are one standard deviation.

The structure-bound water content of the starting crystals was determined by infra-red spectroscopy to be 15 ± 10 H/10^6 Si. The amount of water adsorbed during crushing and centrifuging (and not driven off by drying at 90 °C) onto the surfaces of the freshly-cleaved grains in the three grain fractions to be used for hot pressing was measured by thermogravimetry. Only the finest size fraction showed a resolvable weight loss (of about 0.6%) on heating through 1373 K. This weight loss corresponds approximately to one or two molecular layers of adsorbed water (about 1 nm thickness) on grains of modal size 0.4 μm. The smaller specific surface area of the coarser samples means that an adsorbed water layer would not be expected to produce an unambiguous weight loss signal on heating within instrumental resolution (about 0.1 wt%). It was also determined that heating the quartz powders in air to 1373 K rendered the surfaces hydrophobic, so that they would not take up further water by adsorption from a wet atmosphere.

Deformation experiments were performed on samples prepared from all three size fractions without pre-drying the powders to removed adsorbed water, and also on samples prepared from the 0.4 μm modal size fraction after pre-drying at 1373 K.

3. Experimental methods

3.1. Apparatus

All experiments were performed in a Paterson Instruments argon gas medium testing machine at 300 MPa confining pressure, at temperatures ranging mainly between 1273 and 1473 K. At 300 MPa confining pressure the specimen is expected to be within the β-quartz stability field during compression experiments. The specimen, nominally 1 cm in diameter and 2 cm long, was heated by a 3-zone furnace capable of maintaining temperature constant within better than 10 K along the length of the sample. Temperatures (at the thermocouple position at the top end of the sample) are expected to be correct within ±7 K at 1473 K. Reported experiments include constant displacement rate, constant stress (creep) and stress relaxation tests. Strain rate sensitivity to stress and temperature was determined using stepping tests.

Axial load was applied via a 100 kN servo-controlled electromechanical actuator. External load was measured using a 100 kN Instron load cell, which also provided the calibration standard for a capacitance-type internal load

cell. Resolution of load measurement was within 50 N, but the smallest resolvable load on the sample was influenced greatly by the uncertainties in the load supported by the 0.35 mm wall thickness of iron jacket surrounding the specimen. Spot measurements of jacket strength were made using a copper dummy specimen at 1273 K and found to be reasonably consistent with jacket strengths calculated from the deformation mechanism map for iron (Frost and Ashby, 1982). The iron flow law was therefore used to extrapolate jacket strengths to 1473 K and also to lower temperatures. Thus at 1473 K, about 3 MPa of the apparent stress on a sample at 10^{-4} s^{-1} strain rate is expected to be supported by the jacket, or 5 MPa at 1273 K. Thus if flow stresses fall to the region of 10 MPa, uncertainties in jacket strength begin potentially to have a serious impact on the apparent strength of the quartz sample.

3.2. Specimen hot-pressing and grain growth

Samples were prepared for hot pressing by packing quartz powder into a short iron jacket, 4.5 cm long. The powder was uniaxially cold-pressed in a thick-walled steel split-die to 300 MPa. This pressure is too low to induce significant grain fracture at the grain sizes used (Zhang et al., 1990). The specimen was weighed and measured to allow the starting porosity (typically 45 ± 2%) to be determined. Iron discs of 0.1 mm thickness were placed at the ends of the cylindrical specimen to prevent a reaction between the quartz and the recrystallized alumina loading pistons. The excess iron at the ends of the sample were machined off and the iron-sheathed specimen was loaded into the outer iron jacket, between the two loading pistons, the ends of which were capped off with 3-mm-thick recrystallized alumina discs to protect the piston ends and to prevent extrusion of the sample material up the hollow loading piston bearing the axial thermocouple.

The specimens were not weld-sealed inside their jacket assemblies. However, it is unlikely that any gas or other vapour pressure developed in the pores of the rocks would leak past the iron and alumina discs at each end of the specimen, provided such a pressure was always less than the confining pressure. Any such leakage would show as a pressure rise on the pore pressure gauge, and this was never seen to happen.

Isostatic compaction was carried out in the testing machine immediately prior to mechanical testing. No measurements of the compaction of the specimen could be made during initial pressurization and heating, owing to the changes in the dimensions of the vessel and loading system with pressure and temperature. All samples were given the same compaction procedure, and subsequently taken to the temperature at which they were to be deformed. Compaction was first carried out at 1373 K for 20–24 h, then at 1473 K for a further 3 h. This compaction procedure reduced the porosity to ca. 1% or less for the finest grain sized samples, and 2% or less for the coarsest samples. Except for runs on samples that were terminated immediately after compaction to determine initial porosity reduction and whether any grain growth had occurred, the corresponding residual value of porosity could only be determined by microstructural analysis after the experiment, but this includes also the effects of any further compaction during the subsequent history of non-hydrostatic loading.

Owing to the compaction that occurs during initial heating under pressure and subsequent isothermal, isostatic hot-pressing, the diameter and length of the specimen change. These changes were observed to occur reasonably homogeneously. Thus the effective initial diameter and length of the specimen at the start of the deformation of the specimen were calculated from the porosity loss during hot-pressing.

Grain sizes after experiments were determined using the linear intercept method on polished sections viewed in orientation contrast on the SEM, using lines of a range of orientation to compensate for any preferred grain shape orientation (Table 1). To compare with planar grain diameters, those measured for the starting powders by laser particle sizing must be multiplied by the factor 0.67 (Pannozzo, 1982). Planar grain sizes at the end of experimental runs are plotted against these starting sizes in Fig. 2. Uncertainties for the planar measurements indicated are the standard error on the mean, which is always smaller than the standard deviation that describes the spread of the distribution of particle sizes. All of the hot-pressed and deformed samples (with the exception of non-pre-dried, initially 0.4 μm samples hot-pressed at 1473 K—see below) show slightly larger apparent mean grain sizes than the adjusted laser-sized parent powders, but bearing in

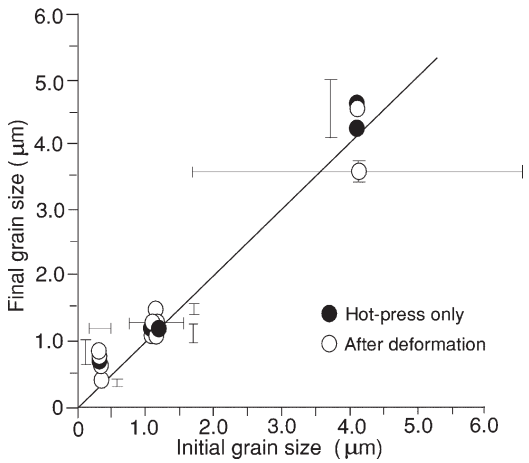

Fig. 2. Relationship between initial (powder) grain sizes and grain sizes either after hot-pressing (black circles) or after deformation (open circles). The 0.4 μm datapoints include both pre-dried and non-pre-dried samples: all others were non-pre-dried. Final grain sizes were measured by linear intercepts on two-dimensional sections. Mean grain sizes of starting powders are multiplied by 0.67 to correspond to their expected mean size in a two-dimensional section. Horizontal error bars are 1 standard deviation of grain-size distribution, vertical error bars are 1 standard deviation on the mean grain size, and hence appear smaller.

Table 1
Summary of test conditions and results for each sample. Mechanical data are presented graphically in Figs. 3–6. Differential stress and strain rate values are given for the strains indicated. Error values on grain size are standard deviation on the measured mean grain size. Confining pressure was 300 MPa

Sample no.	Grain size (μm)/porosity%	Time at temperature (h)	Strain rate (s^{-1})	Flow stress (MPa)	Temperature (K)	Strain (%)	History
Starting grain-size 0.4 micron							
(a) Not pre-dried							
Q8	0.45 ± 0.2	46.6	4.5×10^{-5}	331	1373	6.2	Constant strain rate + stress relaxation
	<1%		2.8×10^{-4}	510	1373	10.0	
			1.9×10^{-5}	410	1373	19.5	
Q22	–	74.6	1.3×10^{-6}	230	1373	1.8	Constant stress-stepping
			2.0×10^{-6}	260	1373	3.3	
			3.0×10^{-6}	310	1373	7.0	
			7.0×10^{-6}	360	1373	13.0	
Q15a	0.64 ± 0.05	71.8	–	–	1373	–	Compaction only
	<1%						
(b) Pre-dried							
Q24	0.61 ± 0.05	30.2	5.0×10^{-5}	465	1473	11.0	Constant strain rate.
	<1%						
Q25	0.74 ± 0.05	27.3	4.8×10^{-5}	570	1373	5.0	Strain rate + T stepping
	<1%		2.0×10^{-4}	455	1473	10.0	
Q26	0.89 ± 0.2	32.0	2.8×10^{-7}	130	1473	4.0	Constant stress with T and σ stepping
	<1%		5.0×10^{-6}	260	1473	8.0	
			1.5×10^{-6}	260	1373	11.0	
			7.4×10^{-7}	260	1273	15.0	
			8.0×10^{-8}	260	1173	16.3	
			9.0×10^{-9}	260	1073	16.8	
Q29	–	238.0	1.7×10^{-6}	40	1473	1.5	Constant stress with T and σ stepping
		(71.7 above 1273 K)	1.8×10^{-5}	310	1473	5.8	
			3.0×10^{-6}	125	1473	7.5	
			2.5×10^{-7}	125	1273	9.0	
			8.0×10^{-7}	250	1273	10.5	
Starting grain-size 1.3 micron							
Q1	1,36 ± 0.09	5.3	–	–	1373	–	Compaction only
	3.9%						
Q2	1.36 ± 0.09	24.0	–	–	1373	–	Compaction only
	3.5%						
Q15b	1.26 ± 0.3	71.8	–	–	1373	–	Compaction only
Q13b	1.23 ± 0.2	66.2	–	–	1473	–	Compaction only
	(approximately 3%)						
Q3	1.10 ± 0.3	47.3	3.2×10^{-5}	440	1373	5.5	Constant strain rate + stress relaxation
	(approximately 3%)						
Q4	–	50.6	4.0×10^{-5}	583	1373	20.6	Constant strain rate + stress relaxation
Q5	1.19 ± 0.05	22.9	3.5×10^{-5}	300	1473	6.0	Constant strain rate + stress relaxation
	1.1%		1.0×10^{-4}	432	1473	10.0	
			1.5×10^{-5}	436	1473	16.9	
Q11	1.78 ± 0.31	54.6	1.0×10^{-6}	160	1473	11.5	Constant strain rate stepping
			1.0×10^{-5}	450	1473	16.6	
Q12	–	47.1	2.4×10^{-4}	539	1473	7.1	Const. strain rate + stress relaxation
Q17	1.16 ± 0.07	32.6	4.0×10^{-5}	502	1473	13.1	Constant strain rate + stress relaxation
	0.97%						
Q28	1.62 ± 0.21	29.0	3.5×10^{-7}	60	1473	14.0	Constant stress stepping
	2.8%		1.9×10^{-6}	120	1473	15.0	
Q31	1.22 ± 0.2	143.6	2.0×10^{-4}	112	1473	2.0	Stress relaxation at small strain
Starting grainsize 4.5 micron							
Q13c	4.76 ± 0.4	66.2	–	–	1473	–	Compaction only
Q15c	4.23 ± 0.3	71.8	–	–	1373	–	Compaction only
Q6	4.52 ± 0.42	20.5	3.6×10^{-5}	419	1473	4.5	Constant strain rate + stress relaxation
	0.47%		2.5×10^{-4}	610	1473	13.5	
Q27	3.57 ± 0.15	184.3	3.4×10^{-5}	550	1473	4.5	Constant strain rate + stress relaxation
	2.0% ± 1.1		5.5×10^{-7}	215	1473	6.7	Constant stress
			6.6×10^{-8}	100	1473	6.8	Constant stress
			2.9×10^{-8}	35	1473	6.9	Constant stress
			1.1×10^{-6}	350	1473	7.0	Constant stress

mind the natural spread of particle sizes in the starting materials and the different times at different temperatures experienced by the various samples, there is no systematic pattern of significant grain growth. Hence no corrections for grain size changes with time during the course of deformation experiments have been applied. For the purpose of relating the sensitivity of flow stress to a single measure of grain size in a flow law, the mean of the particle size measurements derived from each size fraction after the experiments has been used are, respectively, 0.65, 1.3 and 4.0 μm.

The lack of grain growth observed in these experiments is noteworthy given the high temperatures used, but in the starting powders there was contamination in the form of nanometric-sized particles of tungsten carbide introduced during grinding. These could sometimes be seen in the SEM as bright spots around grain boundaries, and tungsten X-ray peaks were occasionally observed around grain boundaries. Small grains of iron oxide were also seen, thinly dispersed throughout the samples but particularly close to the iron jacket. We suspect that this fine dispersion of second phase particles has been responsible for inhibiting grain growth.

Only in the case of initially 0.4 μm samples that were not pre-dried but hot-pressed at 1473 K was a strikingly different behaviour from all other samples and hot-pressing temperatures observed. Even after only a few hours hot-pressing, uniform grain growth to between 10 and 20 μm occurred, bypassing intergranular impurities that otherwise would cause pinning. It is inferred that this was facilitated by pore water pressure transiently developed from the 0.6 wt% of adsorbed water on the grain boundaries, some of which became incorporated as structure-bound water as the migrating grain boundaries swept through the aggregate. These samples were subsequently found to be mechanically weak and deformed readily by intracrystalline plasticity and their behaviour was described in Rutter and Brodie (2004). Hot-pressed 0.4 μm samples that were pre-dried in air at 1373 K did not display this rapid grain growth behaviour, hence pre-drying was necessary to be able to carry out deformation tests on 0.4 μm samples at 1473 K, whilst retaining their fine grain size.

3.3. Deformation experiments

All samples were initially loaded at a constant axial displacement rate that corresponded to strain rates in the range 10^{-7}–10^{-3} s^{-1}. During such an experiment the instantaneous strain rate progressively increases. This is because the specimen progressively becomes shorter, and also because during initial loading a proportion of the applied displacement rate is used to distort the testing machine, according to its compliance. These effects do not influence the apparent rheological behaviour when the flow stress is relatively insensitive to strain rate, but for grain size-sensitive flow, where viscous behaviour is expected to be nearly Newtonian, the instantaneous flow stress can vary considerably due to true strain rate changes occurring as strain accumulates. The expected effects are an apparently enhanced rate of strain hardening and a diffuse apparent yield point. These are considerable effects on the shape of the stress/strain curve that must be taken into account during data interpretation. The apparent strain hardening observed in these experiments can be explained by these effects.

Most tests were punctuated or terminated by stress relaxation experiments (Rutter et al., 1978), in which the motor drive is stopped, and the stored elastic energy in the machine plus specimen is slowly dissipated by creep in the specimen, over a small but not infinitesimal increment (1–2%) of strain. Provided the machine plus specimen compliance is known, the stress relaxation behaviour can be recast as stress versus strain rate, which gives a rapid evaluation of rheologic response on a single test specimen. Strain rate stepping tests, in which the change in flow stress arising from a sudden change in deformation rate is observed, and stress-stepping in creep mode, were also used to help assess the stress sensitivity to strain rate behaviour.

Although most tests were run at constant temperatures of 1373 or 1473 K, a number of temperature-stepping tests were performed in order to assess the strain rate sensitivity to temperature. Such tests can be used to determine the apparent activation enthalpy for flow, which is an essential parameter in the constitutive flow law and is required to extrapolate high temperature behaviour to low temperature, low strain-rate conditions.

In the experimental apparatus used, the specimen with its two loading pistons forms a laterally unsupported slender column, about 250 mm long where it passes through the furnace. Some experiments were therefore troubled by buckling or kinking instabilities in the specimen, which is detectable when the internal and external force gauge traces deviate from parallelism. This meant that several experiments could not be taken to strains exceeding about 16% (although some were taken to over 20% axial shortening). Inhomogeneous deformation above 15–20% shortening also means that mechanical data become progressively more unreliable at higher strains.

At the end of their deformation history, all specimens were rapidly offloaded and quenched at a rate determined by the thermal properties of the furnace. From 1473 K, samples cooled by 200 K in the first minute, and reached 800 K about 5 min later. Beyond this time any further microstructural adjustment is unlikely. During this time, confining pressure dropped by about 50 MPa from 300 MPa.

Data processing involved correction of the measured actuator displacement for the amount of axial machine distortion, correction for the change in cross-sectional area of the specimen with strain (but assuming homogeneous deformation), and for the proportion of the load supported by the iron jacket. The first and third of these are affected by furnace temperature.

4. Experimental results

4.1. Mechanical data

Table 1 lists the experimental conditions of all of the samples tested, together with stresses and strain rates for deformed samples and HIP conditions for samples only heat treated to determine grain growth and porosity loss before deformation. Figs. 3–6 present the mechanical data in graphical form. In all tests the samples behaved wholly ductily and deformed fairly homogeneously. There was never any localization of strain or any sign of brittle deformation. There was also no evidence for bulging of the specimen jacket, which would have arisen had pore pressures built up to a level commensurate with the confining pressure.

For the initially 0.4 μm deformed samples it was expected that those pre-dried and deformed at 1473 K might behave differently from those containing water adsorbed on the grain boundaries. But, bearing in mind some inevitable degree of variability in flow stress between different specimens, it was concluded that they displayed no significant difference in behaviour when deformed at the same temperature, hence the results are presented graphically grouped together. The data are, however, kept separate in Table 1. Infra-red determinations of water content after deformation were made on samples Q31 (1.3 μm, not pre-dried) and Q25 (0.4 μm, pre-dried), giving bulk water contents, respectively, of approximately 1.7 and 2 times greater than the starting material, although these values are not significantly different to that of the starting crystals, given measurement uncertainties. Thus whilst the drying in air of sample Q25 probably removed most of the grain surface water, it apparently has not affected the intragranular water content.

Constant displacement rate stress–strain curves tended to show weakly developed yield points followed by apparent strain hardening (Fig. 3), and Fig. 4 shows creep

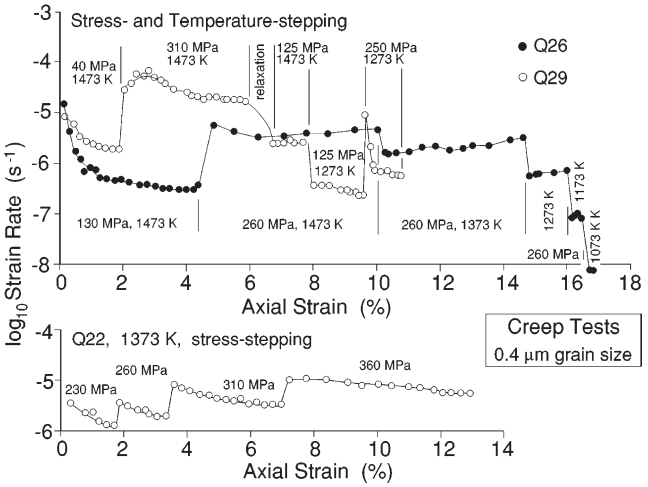

Fig. 4. Constant stress (creep) data for samples prepared from 0.4 μm quartz powder, both pre-dried and non-pre-dried (see Table 1). Creep curves show straining intervals separated by stress and temperature stepping.

data with stress stepping for samples Q22 and Q29. Data in Fig. 5 show how strain rate and flow stress are related. Below about 200 MPa flow stress of all samples show approximately linear viscous behaviour, with coarser-grained samples flowing at lower strain rates at a given stress level. Above about 200 MPa differential stress, the rheology corresponds approximately to a stress exponent of about four or five, although this may not be very meaningful owing to the substantial amount of strain hardening seen at high flow stress levels, and the fact that the flow stress exceeded the confining pressure.

The sensitivity of flow rate to temperature change at constant stress was investigated mainly via temperature-stepping tests at constant stress in creep tests (Fig. 6) and on samples of initial grain size 0.4 μm. These data correspond to an average activation enthalpy for flow of 220 ± 55 kJ/mol between flow stresses of 125 and 310 MPa, with some indication that it decreases towards higher flow stresses.

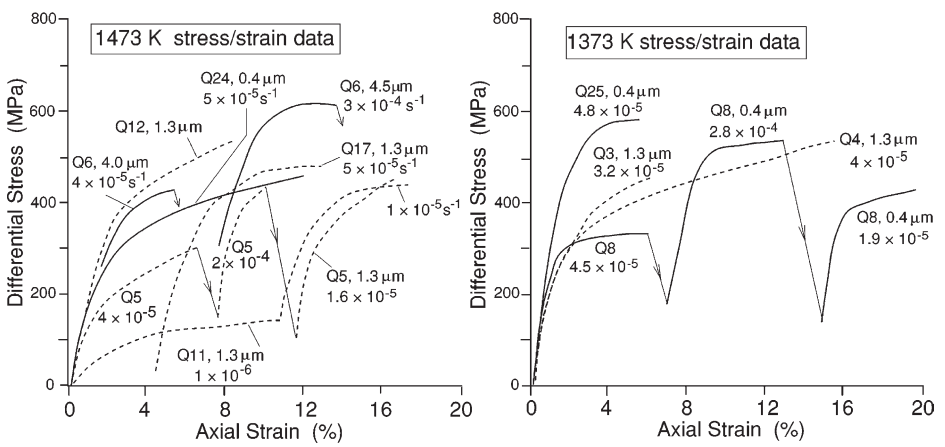

Fig. 3. Stress/strain curves for samples deformed at 1373 and 1473 K. 0.4 μm samples deformed at 1473 K were pre-dried. Grain sizes are indicated by the initial quartz powder size. Strain rate is shown with each curve. Negative slope lines with arrowheads represent stress relaxation intervals.

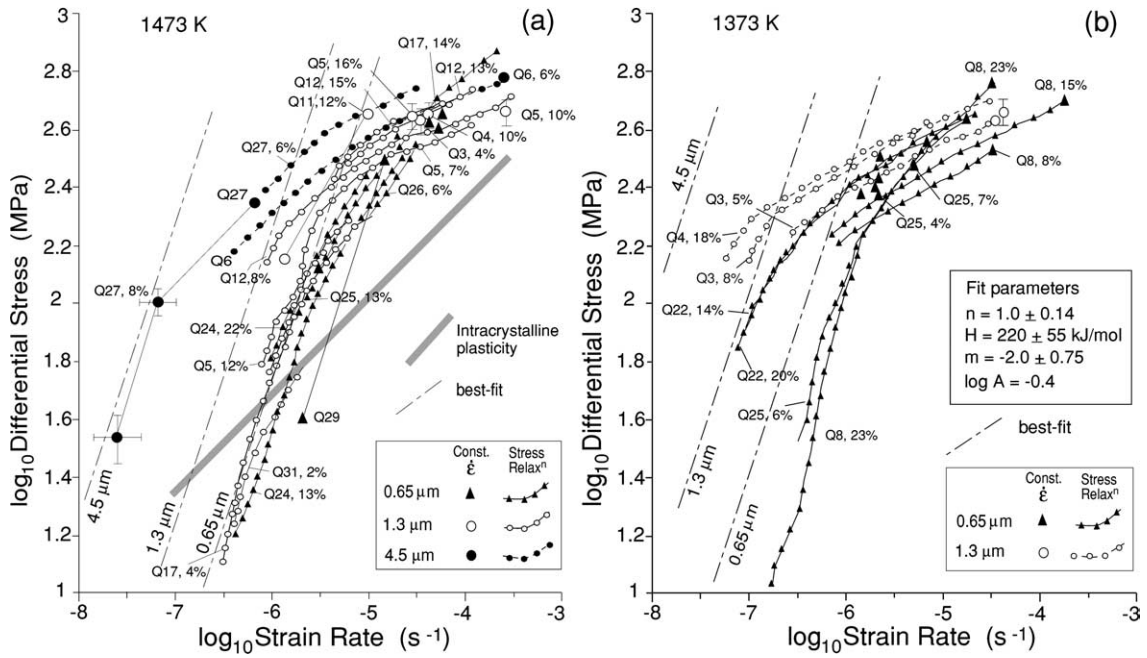

Fig. 5. Summary diagram showing constant strain rate and constant stress data (larger symbols) and stress relaxation (smaller symbols) at (a) 1473 K and (b) 1373 K. Dashed lines are best-fit flow law with a stress exponent of unity and an activation enthalpy of 220 kJ/mol for the planar grain sizes indicated. Grain sizes shown are means for deformed samples. Grey line in (a) shows, for comparison, the best fit for deformation by intracrystalline plasticity of initially non-pre-dried 0.4 μm particle size samples that had undergone grain growth at 1473 K to ca. 15 μm (Rutter and Brodie, 2003).

An estimate was made of the sensitivity of strain rate at constant stress (1 MPa) and temperature (1473 K) to grain-size for the low stress data by extrapolation from the centroid of each data group using $n = 1$ and the average activation enthalpy of 220 kJ/mol, to produce Fig. 7. The data are consistent with a strain rate ($\dot{\epsilon}$) sensitivity to grain size (d) of the form $\dot{\epsilon} \propto 1/d^m$, where m is closer to two than to three, although a best-fit value is not well constrained. If we assume that on theoretical grounds the true values for n and m, respectively, are exactly one and two, and that the flow law for grain-size sensitive flow is of the form $\dot{\epsilon} = A\sigma^n \exp(-H/RT)/d^m$ (stress in MPa, grain size in microns), then a set of best-fit parameters with these constraints would be $\log A = -0.4 \pm 2.1$, $n = 1.0 \pm 0.14$, $m = 2.0 \pm 0.75$ and $H = 220 \pm 55$ kJ/mol.

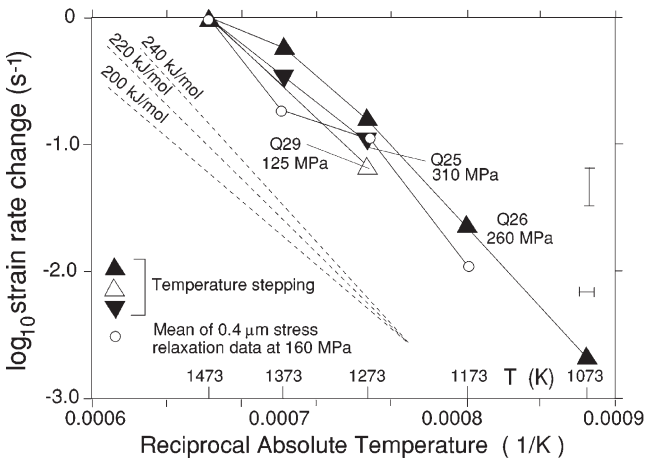

Fig. 6. Results of temperature stepping experiments (specimen number indicated) at different constant stress levels (indicated). Strain rate changes are shown with reference to the strain rate at 1473 K. Mean differences between stress relaxation data at constant stress are also shown. Dashed lines show reference slopes corresponding to different activation enthalpy values. The data points collectively are best represented by 220 kJ/mol.

4.2. Microstructural observations

Samples were studied using optical microscopy, scanning electron microscopy (SEM) and high-voltage (300 kV) transmission electron microscopy (HVTEM). Owing to the fine grain size of these samples, grain shapes could only be seen in the SEM using orientation contrast. Porosity was estimated from pore areas measured on the images (Table 1). For the 0.4 μm samples, porosity was always less than

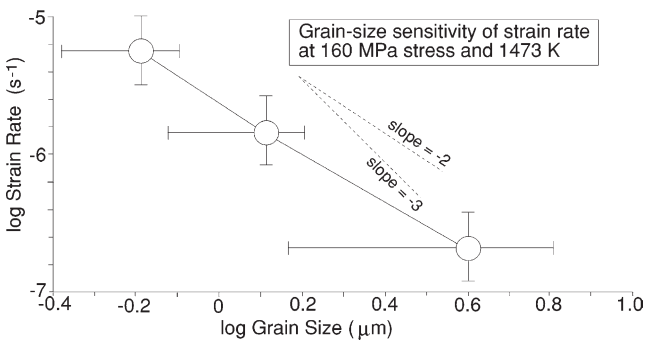

Fig. 7. Sensitivity of strain rate at 160 MPa flow stress to grain size at 1473 K. The mean values are best represented by a slope of −2, although the uncertainty bars (1 standard deviation) indicate that the slope is not well constrained.

about 1% and was not resolvable quantitatively. Residual porosity in the 1.3 and 4.5 μm samples ranged up to 2%. Grain size (Table 1) was estimated from linear intercept counts on a range of variously oriented lines on each image. X-ray crystallographic preferred orientation determinations were also carried out on three of the experimentally deformed samples (Fig. 8).

It should be borne in mind that, because of stress and temperature stepping and stress relaxation cycles imposed on most samples, they have generally suffered complex deformation histories over a wide range of stresses, and that this might be expected to be reflected in their microstructural characteristics. Most specimens, however, were exposed to the lowest stresses of their histories for at least 1% strain prior to offloading and quenching.

Images of experimentally deformed samples are shown in Fig. 9. Fig. 9a shows an example of an orientation contrast image (sample Q25, starting grain size 0.4 μm, pre-dried, shortened 13%). Deformed samples consistently displayed an equigranular microstructure, with no apparent relation between grain shape and finite strain. In the HVTEM, dislocations were near absent in the sub-micron grains and grains were equant (Fig. 9b). However, samples that had been quenched from high stresses (e.g. >200 MPa) or relatively large grains (e.g. >2 μm) in any given sample showed diffraction contrasts indicative of a wide range of dislocation densities (Fig. 9c and d). Gas bubbles were absent, except occasionally on grain boundaries, and no rapid electron beam damage was noted, suggesting that any diffusive introduction of water into the quartz did not lead to supersaturation. There was no discernible microstructural difference between the pre-dried and non-pre-dried (that had not been taken above 1373 K during hot-pressing and hence did not undergo rapid grain coarsening) 0.4 μm samples in the SEM, but pre-dried samples were not studied using the HVTEM. No evidence of grain boundary melting was seen in any samples.

Inverse pole figures (Fig. 8) of three samples, deformed to strains ranging between 12 and 20%, showed no significant development of crystallographic preferred orientation relative to the uniform orientation distribution of the starting material.

5. Discussion and geological implications of results

5.1. Deformation mechanisms

Below a differential stress of about 200 MPa for the 0.4 μm samples, decreasing to about 100 MPa for the 4.5 μm samples, all test pieces displayed fully ductile, linear viscous flow, coupled with maintenance of a fine, equigranular microstructure, lack of development of grain shape fabric or crystallographic preferred orientation (bearing in mind the low strains) and a lack of evidence for dislocation activity within the finest, best equilibrated grains. They also displayed grain-size sensitive flow, such that strain rate at constant stress varies as the reciprocal grain diameter squared. These characteristics suggest strongly that deformation occurred by high-temperature grain-boundary sliding controlled by volume diffusion at stress levels below 100–200 MPa. Although the effects of varying confining pressure were not investigated, flow at differential stresses substantially below the confining pressure is believed to imply that cataclasis or other dilatation producing processes did not contribute to the deformation.

The evidence of significant dislocation activity, particularly in the 4.5 μm samples and in the coarser grains within the 1.3 and 0.4 μm samples, and the non-linear flow behaviour at stresses above 100–200 MPa, indicates that intracrystalline plastic flow was active. For those samples deformed at differential stresses above 300 MPa, it is possible that there was some additional contribution to the flow from cataclastic processes.

As pointed out earlier, we found that the initially 0.4 μm size fraction, when not pre-dried and thus bearing ca. 0.6 wt% adsorbed water on grain boundaries, underwent

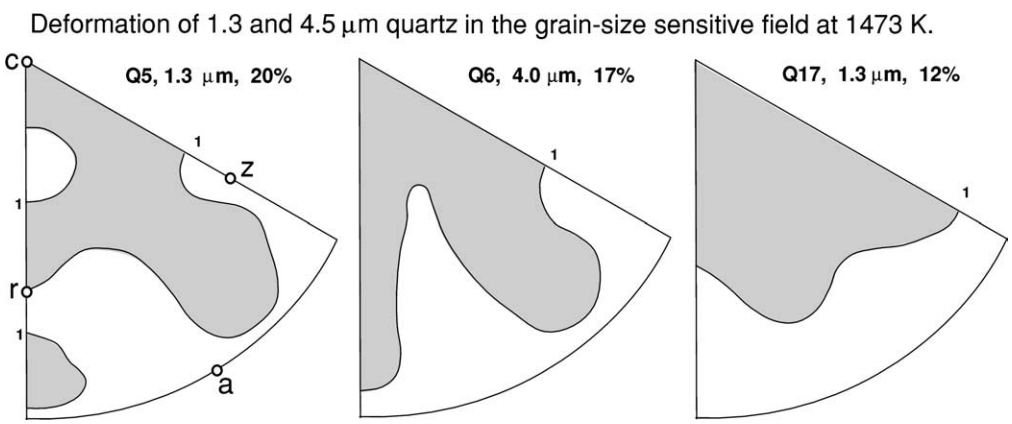

Fig. 8. Inverse pole figures showing the preferred orientation of the compression direction, determined by X-ray texture goniometry, for three samples experimentally deformed at 1473 K (grain sizes and strains indicated, densities as multiples of uniform distribution, crystallographic forms indicated on the Q5 figure).

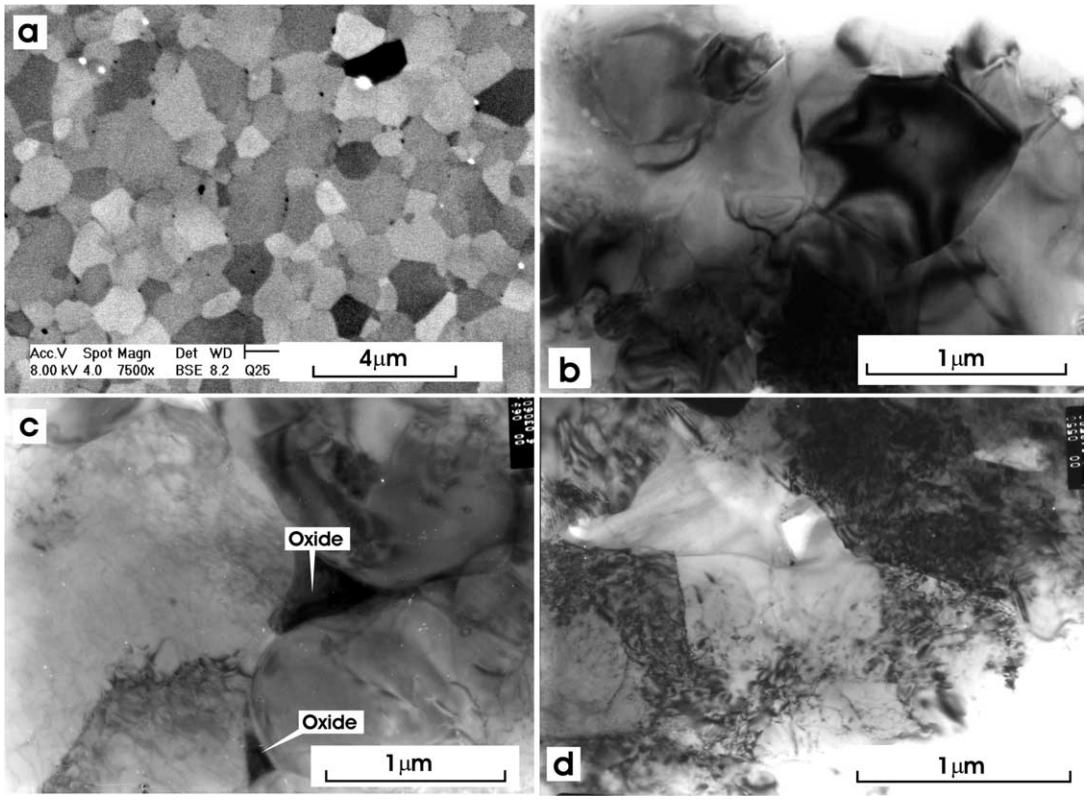

Fig. 9. Microstructures of experimentally deformed samples. (a) Orientation contrast image SEM of sample Q25, pre-dried, prepared from 0.4 μm quartz powder, deformed 13% at 1473 K. Grains are equant and well-equilibrated, with near-zero porosity. Bright white spots are iron oxide or tungsten carbide particles. (b) HVTEM image of sample Q8, not pre-dried, prepared from 0.4 μm quartz powder, deformed 23% at 1373 K, finishing stress relaxation at 10 MPa differential stress. Grains are equant and dislocation-free. (c) HVTEM image of some larger grains in sample Q8, showing some dislocation density. Iron oxide grains produced from reaction between adsorbed water and the iron jacket are seen at triple points between grains. (d) HVTEM image of sample Q6, prepared from 4.5 μm quartz powder and deformed 14% at 1473 K, entirely at differential stresses above 100 MPa. There is a heterogeneously distributed high density of dislocations.

rapid grain growth to about 15 μm grain size when hot-pressed at 1473 K, and could be deformed by intracrystalline plasticity with a stress exponent of 3.0 (Rutter and Brodie, 2004). On Fig. 5a we show the trend of the rheological behaviour of these coarsened samples for comparison with the fine-grained samples described in this paper. All the fine-grained samples are substantially stronger at high strain rates than the 15 μm samples and appear to deform with a larger stress exponent. For deformation by intracrystalline plasticity, finer grained quartz rocks are normally expected to be stronger than coarser grained rocks at the same temperature, strain rate and water fugacity.

5.2. Water content

No water was added to any of the specimen assemblies prior to testing. The only water present was that which was adsorbed onto the surfaces of the quartz grains during grinding plus the small amount of structure-bound water initially present in the starting material. Adsorbed water content would be greatest (0.6 wt%) for the 0.4 μm grain-size specimens that were not pre-dried. The development of pore pressure and the activity of the components of the vapour phase from the dehydroxylation of grain surfaces depends on sample porosity collapse, temperature, the reaction between water and the iron jacket to produce iron oxide and hydrogen (Fig. 9c), and the natural dissociation of water. Based on the initial water contents, the temperatures attained and the pore collapse history, calculated pore pressure during compaction in the experiments reported here is not expected to have transiently exceeded 100 MPa in the initially non-pre-dried 0.4 μm samples that were hot pressed at only 1373 K, and about 20–50 MPa in the 1.3 and 4 μm samples, progressively becoming lowered according to the amount of reaction with the iron jacket. The accelerated grain growth that was seen in the non-pre-dried 0.4 μm samples hot-pressed at 1473 K is believed to have arisen owing to the production of pore water pressure transiently approaching the confining pressure.

Post and Tullis (1998) reported that at about 1150 K and 1.5 GPa confining pressure, water was able to diffuse up to 15 μm into large quartz grains and cause dislocation recovery microstructures to develop near the grain boundaries. The implication seems to be that under the conditions of our experiments on finer grained samples, although at a

water fugacity at least 10 times lower (the fugacity coefficient of water around 300 MPa and 1373 K is very close to unity), some degree of diffusion of water into the quartz is to be expected, depending on the evolution of pore pressure developed during hot-pressing, and this would favour the observed intracrystalline plasticity at differential stresses above 200 MPa. The likely variability in water fugacity (20–100 MPa) to which different samples were exposed does not seem to have produced any corresponding variations in mechanical behaviour above the non-systematic scatter seen in the experimental data.

5.3. Deformation rate control

For grain size-sensitive flow involving grain boundary sliding with accommodation by diffusion or dislocation motion it is possible to derive a number of theoretical constitutive flow laws, in which the values of all parameters are predicted (e.g. Kashyap and Mukherjee, 1985). These vary according to the geometric details of the model and the inferred rate-controlling process. The simplest such model is that of Ashby and Verrall (1973), and it is the only one for which the accommodation mechanism for sliding is diffusion alone. It predicts linear-viscous behaviour, in correspondence with observations from our experiments. Other models invoke varying degrees of accommodation by intracrystalline plasticity and predict more non-linear viscous flow. For the Ashby–Verrall model with accommodation by intragranular (volume) diffusion, the grain-size exponent is expected to be two, as observed here. The theoretical constitutive law for uniaxial strain in a single phase material is:

$$\dot{\epsilon} = 100 V \sigma D_v / RTd^2 \quad (1)$$

in which V is the solid phase molar volume and D_v is the volume diffusion coefficient for the slowest diffusing species, and includes the Arrhenius temperature dependence.

Many studies of self-diffusion in quartz have been carried out, under both hydrothermal and dry conditions, and a wide range of diffusion parameters have been obtained (see compilations by Freer (1981) and Brady (1995)). The oxygen volume diffusion data by gas/solid exchange under dry conditions, apparently closest to the present experiments, are those of Haul and Dümbgen (1962), using a gas–solid isotopic exchange at 1273–1473 K. They reported D_o ($= D_v$ at $1/T = 0$) $= 3.7 \times 10^{-13}$ m^2 s^{-1} with $H = 230$ kJ/mol (within experimental error identical to the H value from the deformation experiments reported here), although they suggest that D_o is probably too low by a factor of $\times 10$ because their nominal value does not take account of surface roughness of their powdered samples. Dry oxygen diffusion data for quartz are substantially slower than under 'wet' conditions at the corresponding temperature, depending on the water fugacity (Dennis, 1984; Gilletti and Yund, 1984; Farver and Yund, 1991). Applying the dry oxygen diffusion parameters to Eq. (1) does predict fairly closely the results of our experiments (Fig. 10), however.

Jaoul et al. (1995) reported silicon volume diffusion data in very pure (<0.1 H/10^6 Si) quartz under dry conditions between 1670 and 1870 K. With an activation enthalpy of 746 kJ/mol, silicon volume diffusion is several orders of magnitude slower than oxygen diffusion in dry quartz over the temperature range of our experiments. They inferred that diffusion was due to the motion of intrinsic silicon interstitials. We would normally expect, therefore, that silicon diffusion would control the rate of diffusion creep in quartz that is sufficiently pure for thermally-produced defects to dominate. But such creep would be very much slower than observed here and display a correspondingly high value of activation enthalpy.

Hobbs (1984) pointed out that the presence of (OH)-related defects in the quartz structure increases the concentration of charged oxygen vacancies [$V_{o^{\cdot\cdot}}$] and silicon interstitials [$Si^{////}_I$] when the impurity is present in sufficient concentration to exceed the concentrations of intrinsic (thermally-produced) defects, and hence enhances the diffusivity of the above species. For the charge neutrality range controlled by a water-related defect such as $2[V_{o^{\cdot\cdot}}] = [(HOH)^{\prime}_I]$ (Kroger–Vink notation), [$V_{o^{\cdot\cdot}}$] increases as

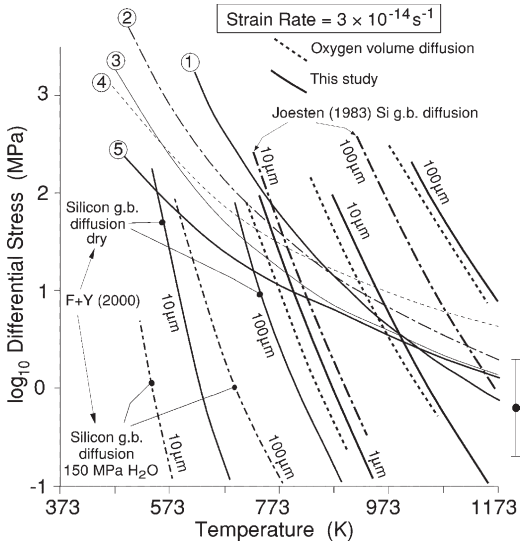

Fig. 10. Extrapolation of experimental data to a geological strain rate of 3×10^{-14} s^{-1}. Curves labelled 1–5 are for intracrystalline plasticity referred to a water fugacity of 300 MPa: 1. Rutter and Brodie (2003); 2. Gleason and Tullis (1995); 3 and 4. Luan and Paterson (1992), gel origin and silicic acid origin, respectively; 5. Hirth et al. (2001). Six curves on the right show extrapolation from diffusion creep data of this study (solid lines) and calculated from the diffusion creep law of Ashby and Verrall (1973) assuming dry oxygen diffusion is rate controlling (dashed lines). Leftmost four curves show grain boundary diffusion creep behaviour calculated from the silicon diffusion data of Farver and Yund (F + Y (2000)) for dry conditions (solid lines) and at 150 MPa water pressure (dashed lines). Dash–dot curves show extrapolation for grain-boundary diffusion creep using Si g.b. diffusion law based on natural grain growth kinetics (Joesten, 1983). Grain sizes indicated with each diffusion creep curve. Error bar on extrapolation indicated far right.

$f(H_2O)^{2/3}$ and $[Si''''_I]$ increases more rapidly, as $f(H_2O)^{4/3}$, but it is not clear whether the more rapid increase would be sufficient for silicon diffusivity to overtake oxygen diffusivity in the temperature range of interest. The effect of the enhancement of diffusivity and hence of diffusion creep in polycrystalline oxides through increase in point defect concentrations as a result of doping with aliovalent impurities has been demonstrated for magnesia, alumina and titania (review by Gordon (1984)). Similarly, Mei and Kohlstedt (2000) attributed the enhancement of diffusion creep in wet samples of fine-grained polycrystalline olivine to an increase in concentration of extrinsic silicon interstitials according to the concentration of water-related defects.

To explain the apparent correlation of our creep results with dry oxygen diffusion data it would be necessary to assume that a water fugacity probably around 20–50 MPa would be able to raise the silicon interstitial diffusivity to a level greater than that for oxygen defects over the temperature interval of interest. Further, the Haul and Dümbgen (1962) oxygen data would have to have been acquired in samples for which oxygen defect concentrations were controlled by impurity concentrations. It seems unlikely that either would be true, because oxygen diffusivity under hydrothermal conditions is several orders of magnitude faster than under dry conditions, depending on the water fugacity (Dennis, 1984; Gilletti and Yund, 1984; Farver and Yund, 2000). Alternatively, the correlation with the dry oxygen diffusion data may be fortuitous and the creep may indeed be controlled by extrinsic silicon defect diffusion, with the H lower and D_o higher than for pure quartz because the defect formation energy does not have to be supplied in this case. Unfortunately, no data are available for silicon volume diffusion in quartz under hydrothermal conditions, and technical issues mean that such data will be extremely difficult to obtain (R. Yund, pers. comm. 2003). Nevertheless, it seems most likely that extrinsic silicon diffusion controls creep in our experiments.

5.4. Geological implications

Fig. 10 shows the result of extrapolating the experimental flow law data for the fine-grained samples deformed in the grain size-sensitive regime to a 'natural' geological strain rate of 3×10^{-14} s^{-1}. The effect of the extrapolation of the estimated experimental errors is also shown. These data are believed to correspond to a maximum of 100 MPa water fugacity and an oxygen fugacity controlled by the oxidation of the iron jacket. Water fugacity for quartz deformation in nature would probably be about 2–4 times higher than this, and would likely produce some acceleration of creep rate, perhaps by the same factor. This extrapolation is subject to the assumption that the flow law parameters determined for the experimental conditions do not change over the range of the extrapolation. Corresponding extrapolation of the flow laws for intracrystalline plastic flow of quartz of Luan and Paterson (1992), Gleason and Tullis (1995), Hirth et al. (2001) and Rutter and Brodie (2004) are also shown for comparison. All the latter refer to a water fugacity of 300 MPa assuming a water fugacity exponent in their respective flow laws of unity.

The most striking feature of the extrapolation is that it predicts that, even for very fine-grained aggregates, rather high temperatures are required to induce grain-size sensitive flow (800–900 K for grain sizes of 1 μm or higher). In nature, very fine grained (a few microns) quartz mylonites are commonly found in rocks that have been deformed and metamorphosed in the greenschist or amphibolite facies (600–800 K). For flow to occur in nature by a grain-size sensitive process such as volume diffusion creep, H would have to become lower at temperatures below the experimental range (for example if diffusion were to become controlled by a different point defect regime), or the water fugacity would have to be very substantially higher, or there might be a transition at lower temperature to grain-boundary diffusion control, with attendant lowering of D_o and H and the development of an enhanced sensitivity of strain rate to grain size. Combinations of high temperature and high water fugacity in nature mitigate against grain size-sensitive flow because they tend to favour grain growth, which in turn can be inhibited if intergranular pinning impurities are present.

Consistent with the apparent difficulty of diffusion-controlled, grain-size sensitive creep in nature, in a study of very fine-grained (< 10 μm) quartz mylonites from central Australia, Fliervoet and White (1995) found microstructural evidence (dislocation activity, subgrains and a strong crystallographic preferred orientation) that, despite the marked tectonic grain-size reduction, deformation by grain boundary sliding processes did not occur and flow continued to be dominated by dislocation creep with the very fine equidimensional grain size being maintained by continuous dynamic recrystallization. Their study and our extrapolation of experimental data, therefore, indicate that the mere observation of tectonic grain size reduction and equidimensional grains may not of themselves imply linear viscous flow by diffusion-accommodated grain boundary sliding. On the other hand, Behrmann and Mainprice (1987) cited microstructural evidence of cavitation and lack of crystallographic preferred orientation supporting the inference of grain size sensitive flow in a quartzofeldspathic mylonite.

The lower H and higher D_o typically associated with grain boundary diffusion, together with the greater sensitivity of flow rate to grain size ($\dot{\epsilon} \propto d^{-3}$), may lead to grain-boundary diffusion controlled creep at geologically significant temperatures. Farver and Yund (2000) report silicon grain boundary diffusion kinetics for quartz at 150 MPa water pressure, giving $D_{bulk}(T)$ (m^2 s^{-1}) $= 3.7 \times 10^{-10} \exp(-137 \pm 18$ kJ/R$T)$, where $D_{bulk} \sim D_{gb}\delta/d$, in which D_{gb} is grain boundary diffusivity, δ is grain boundary effective thickness and d is grain

diameter (1.2 μm). Under dry conditions, they obtained $D_o = 6.2 \times 10^{-9}\ m^2\ s^{-1}$ and $H = 178 \pm 38$ kJ/mol. Taking Eq. (1) modified for grain-boundary controlled diffusion creep (following Ashby and Verrall (1973)), and with $\delta = 2$ nm, calculated flow stresses for a strain rate of $3 \times 10^{-14}\ s^{-1}$ by silicon grain boundary diffusion-controlled creep are shown in Fig. 10 for both the dry and wet cases, and compared with the extrapolation of our experimental data. These extrapolations imply that, over a wide range of grain sizes and metamorphic conditions encountered in orogenesis, diffusion creep might control the flow to the exclusion of intracrystalline plasticity. The Farver and Yund data also lead to a 10^6 overestimation of strain rate when extrapolated to the temperature and strain rate conditions of our experiments.

Joesten (1983) estimated a silicon grain boundary diffusion law from observations of natural grain growth kinetics in a thermal aureole, and obtained diffusion rates approximately 10^4 slower than Farver and Yund (2000) at comparable temperatures. Using Joesten's diffusion parameters ($D_o = 3 \times 10^{-9}\ m^2\ s^{-1}$ and $H = 190$ kJ/mol) to extrapolate grain boundary-diffusion controlled creep to a strain rate of $3 \times 10^{-14}\ s^{-1}$ yields curves also shown in Fig. 10. This extrapolation lies between those of our experimental data and those of Farver and Yund (2000). The discrepancies between these three groups of data are substantial and they are compounded by contrasting interpretations on the role of grain size sensitive creep from studies on naturally deformed rocks. The way forward requires experimental deformation studies on fine-grained quartzites under wet conditions, to test the predictions of rapid grain boundary-diffusion creep arising from the diffusion data of Farver and Yund (2000).

6. Summary and conclusions

Synthetic, hot-pressed aggregates of ultrafine-grained quartz, with porosities between 0 and 2%, were prepared from crushed single crystals of Brazilian quartz of initial modal grain sizes 0.4, 1.3 and 4.5 μm. These were deformed at temperatures in the range 1273–1473 K, 300 MPa confining pressure. Except for some 0.4 μm samples that were pre-dried by heating in air at 1373 K before hot-pressing, some water was present during deformation, arising from adsorption onto freshly-cleaved grain surfaces during sample preparation, plus the small amount already present structure-bound within the quartz. For all samples, flow at differential stresses below 100 MPa occurred by grain-size sensitive, linear-viscous creep, with an equigranular microstructure being maintained, and no evidence of development of crystallographic preferred orientation for shortening strains up to 20%. Strain rate varies with grain size approximately as d^{-2}, suggestive of rate control by volume diffusion. It is inferred that the grain-size sensitive flow was controlled by silicon diffusion, with the defect concentration dependent on water fugacity. Effective water fugacity was estimated to be finite but below 100 MPa in these experiments, and smallest for the coarser samples. The effect of water fugacity on defect concentration and hence creep rate is anticipated to vary approximately linearly with water pressure but any such effects in the present data are not apparent relative to scatter in the experimental results from other causes. Future experiments will require more careful attention to minimizing non-reproducibility between samples and controlling the activities of components in the vapour phase.

Above approximately 200 MPa differential stress for 0.4 μm samples and 100 MPa for 4.5 μm samples, the flow became non-linear, with a stress exponent of approximately 4–5. In the coarser-grained samples in particular, TEM examination showed evidence of considerable dislocation activity. Cataclastic deformation may also contribute to deformation at the highest differential stress levels.

The larger amount of water (approx. 0.6 wt%) adsorbed onto the 0.4 μm non-pre-dried aggregates caused grain growth of samples to about 15–20 μm at 1473 K in a few hours, and these samples deformed by intracrystalline plasticity at stresses lower than required for intracrystalline plastic flow in all the other samples that did not undergo such grain growth. Adsorbed water could be removed from the crushed quartz powders by heating in air to 1373 K prior to hot-pressing. This prevented grain growth, so that the 0.4 μm samples deformed by grain size-sensitive creep in the same way as the non-pre-dried samples that did not undergo grain growth.

Extrapolation of the flow behaviour for grain-size sensitive creep to a natural strain rate of $3 \times 10^{-14}\ s^{-1}$ predicts that rather high temperatures are needed to activate grain-size sensitive flow, even for very fine grained rocks (e.g. >900 K at a grain size of 1 μm or more). It is possible that changes in flow law parameters occur over the extrapolation range, so that the experimental results might not be relevant to natural deformation of fine-grained quartzite. In particular, rate control by grain boundary diffusion is likely to become dominant at lower temperatures, outside the experimental range. Alternatively, it may be that even strongly grain-refined quartz rocks continue to deform in nature mainly by intracrystalline plastic processes, particularly at low water fugacities, coupled with dynamic recrystallization to reset continuously the microstructure. There is some support for both views from microstructural studies of naturally deformed rocks.

Acknowledgements

This work was supported by UK NERC grant GR3/8627. Experimental Officer Robert Holloway helped maintain the experimental apparatus used in this study. Peter Morris is thanked for carrying out IR analyses, and Martin Casey for performing the X-ray texture determinations on three of our

experimentally deformed samples. The Manchester Materials Science Centre provided HVTEM facilities. Jan Tullis and Greg Hirth are thanked for careful and constructive reviews.

References

Ashby, M.F., Verrall, R.A., 1973. Diffusion accommodated flow and superplasticity. Acta Metallurgica 21, 149–163.

Behrmann, J.H., Mainprice, D.H., 1987. Deformation mechanisms in a high temperature quartz-feldspar mylonite: evidence of superplastic flow in the lower continental crust. Tectonophysics 140, 297–305.

Brady, J.B., 1995. Diffusion data for silicate minerals, glasses and liquids. In: Ahrens, T.H., (Ed.), Mineral Physics and Crystallography, A Handbook of Physical Constants, AGU Reference Shelf, 2., pp. 269–290.

Dell'Angelo, L., Olgaard, D., 1995. Experimental deformation of fine-grained anhydrite: evidence for dislocation and diffusion creep. Journal of Geophysical Research 100, 15425–15440.

Dennis, P.F., 1984. Oxygen self-diffusion in quartz under hydrothermal conditions. Journal of Geophysical Research 89, 4047–4057.

Dimanov, A.G., Dresen, G., Xiao, X., Wirth, R., 1999. Grain boundary diffusion creep of synthetic anorthite aggregates: the effect of water. Journal of Geophysical Research 104, 10483–10497.

Farver, J.R., Yund, R.A., 1991. Oxygen diffusion in quartz: dependence on temperature and water fugacity. Chemical Geology 90, 55–70.

Farver, J.R., Yund, R.A., 2000. Silicon diffusion in a natural quartz aggregate: constraints on diffusion transfer creep. Tectonophysics 325, 193–205.

Fliervoet, T.F., White, S.H., 1995. Quartz deformation in a very fine grained quartzo-feldspathic mylonite: a lack of evidence for dominant grain boundary sliding deformation. Journal of Structural Geology 17, 1095–1109.

Freeman, B., Ferguson, C.C., 1986. Deformation mechanism maps and micromechanics of rocks with distributed grain sizes. Journal of Geophysical Research 91, 3849–3860.

Freer, R., 1981. Diffusion in silicate minerals and glasses: a data digest and guide to the literature. Contributions to Mineralogy and Petrology 76, 440–454.

Frost, H.J., Ashby, M.F., 1982. Pure iron and ferrous alloys. In: Deformation Mechanism Maps, the Plasticity and Creep of Metals and Ceramics, Pergamon, New York, pp. 61–66.

Gilletti, B.J., Yund, R.A., 1984. Oxygen diffusion in quartz. Journal of Geophysical Research 89, 4039–4046.

Gleason, G.C., Tullis, J., 1995. A flow law for dislocation creep of quartz aggregates determined with the molten salt cell. Tectonophysics 247, 1–23.

Goldsby, D.L., Kohlstedt, D.L., 2001. Superplastic deformation of ice: experimental observations. Journal of Geophysical Research 106, 11017–11030.

Haul, R., Dümbgen, G., 1962. Untersuchung der Sauerstoffbewiglichkeit in titandioxid, quarz und quarzglas mit hilte des heterogenen isotope-naustaches. Zeitschrift Electrochemie 66, 636–641.

Hirth, G., Kohlstedt, D.L., 1995. Experimental constraints on the dynamics of the partially molten upper mantle: deformation in the diffusion creep regime. Journal of Geophysical Research 100, 1981–2001.

Hirth, G., Teyssier, C., Dunlap, J.W., 2001. An evaluation of quartzite flow laws based on comparisons between experimentally and naturally deformed rocks. International Journal of Earth Sciences 90, 77–87.

Hobbs, B.E., 1984. The hydrolytic weakening effect in quartz. In: Schock, R.N., (Ed.), Point Defects in Minerals, AGU Monograph, 31., pp. 151–170.

Jaoul, O., Béjina, F., Élie, F., Abel, F., 1995. Silicon self-diffusion in quartz. Physical Review Letters 74, 2038–2041.

Joesten, R., 1983. Grain growth and grain boundary diffusion in quartz from the Christmas Mountains (Texas) contact aureole. American Journal of Science, 283A, 233–255.

Karato, S., Paterson, M.S., Fitzgerald, J.D., 1986. Rheology of synthetic olivine aggregates: influence of grain size and water. Journal of Geophysical Research 91, 8151–8176.

Kashyap, B.P., Mukherjee, A.K., 1985. On the models for superplastic deformation. In: Baudelet, B., Suery, M. (Eds.), Superplasticity. Proceedings of an International Conference on Superplasticity. Editions du CNRS, Paris, pp. 4.1–4.31.

Luan, F.C., Paterson, M.S., 1992. Preparation and deformation of synthetic aggregates of quartz. Journal of Geophysical Research 97, 301–320.

McDonnell, R.D., Peach, C.J., Spiers, C.J., 1999. Flow behavior of fine-grained synthetic dunite in the presence of 0.5 wt% H_2O. Journal of Geophysical Research 104, 17823–17845.

Mei, S., Kohlstedt, D.L., 2000. Influence of water on the plastic deformation of olivine aggregates: 1. diffusion creep regime. Journal of Geophysical Research 105, 21457–21469.

Pannozzo, R., 1982. Determination of size distributions of spheres from size distributions of circular sections by Monte Carlo methods. Microscopia Acta 86, 37–48.

Post, A.D., Tullis, J., 1998. The rate of water penetration in experimentally deformed quartzite: implications for hydrolytic weakening. Tectonophysics 295, 117–137.

Rutter, E.H., Brodie, K.H., 2004. Experimental intracrystalline plastic flow in hot-pressed synthetic quartzite prepared from Brazilian quartz crystals. Journal of Structural Geology 26, 259–270.

Rutter, E.H., Atkinson, B.K., Mainprice, D.H., 1978. On the use of the stress relaxation testing method in studies of the mechanical behaviour of geological materials. Geophysical Journal of the Royal Astronomical Society 55, 155–170.

Rutter, E.H., Casey, M., Burlini, L., 1994. Preferred crystallographic orientation development during the plastic and superplastic flow of calcite rocks. Journal of Structural Geology 16, 1431–1446.

Rybacki, E., Dresen, G., 2000. Dislocation and diffusion creep of synthetic anorthite aggregates. Journal of Geophysical Research 105, 26017–26036.

Tullis, J., Yund, R.A., 1991. Diffusion creep in feldspar aggregates: experimental evidence. Journal of Structural Geology 13, 987–1000.

Walker, A.N., Rutter, E.H., Brodie, K.H., 1990. Experimental study of grain-size sensitive flow of synthetic, hot-pressed calcite rocks. In: Knipe, R.J., Rutter, E.H. (Eds.), Deformation Mechanisms, Rheology and Tectonics, Geological Society Special Publication, 54., pp. 259–284.

Zhang, J., Wong, T.-F., Davis, D.M., 1990. Micromechanics of pressure-induced grain crushing in porous rocks. Journal of Geophysical Research 95, 341–352.